

Revisiting Quantum Sieving of H₂ and D₂ in a Carbon Nanotube: Competition of ZPE Effects and Resonance Enhanced Tunneling

Manel Mondelo-Martell^{*,†,‡} and Fermín Huarte-Larrañaga[‡]

[†]*Institut für Theoretische Physik, Freie Universität Berlin, Berlin*

[‡]*Department of Materials Science & Physical Chemistry and Institute of Theoretical and Computational Chemistry (IQTUCB), Universitat de Barcelona, Barcelona*

E-mail: manel.mondelo@fu-berlin.de

Abstract

Nanoporous materials have the potential to be used as *molecular sieves* to separate chemical substances in a mixture via selective adsorption and kinetic sieving. The separation of isotopologues is also possible via the so-called *quantum sieving* effect: the different effective size of isotopologues due to their different ZPE. Here we compare the diffusion rates of Hydrogen and Deuterium in (8,0) Single Walled Carbon Nanotubes obtained through quantum dynamics methods. The diffusion channels obtained present important contributions from resonances connecting the potential wells. These resonances, which are more important for H₂ than for D₂, increase the low-temperature diffusivity of both isotopologues, but prevent the inverse kinetic isotope effect reported for similar nanostructured systems.

1 Introduction

The importance of hydrogen in chemical research and industry cannot be overestimated: from its use as reagent in synthetic chemistry and several industrial processes, to its potential application as a clean fuel for combustion batteries, the future of our society seems to be inevitably tied to being able to harness hydrogen's capabilities as efficiently as possible¹⁻³. One particular aspect of such harnessing is the separation of hydrogen and deuterium, since the latter has very different applications in the areas of isotopological tracing⁴, proton nuclear magnetic resonance spectroscopy^{5,6}, neutron scattering^{7,8}. If chemical separation processes are extremely costly *per se*, using around 10-15% of the total amount of energy consumed worldwide⁹, isotopological separation is comparatively the most expensive^{10,11}. In the particular case of H₂/D₂ separation, at industrial level the most common technique is the cryogenic distillation, which achieves a separation factor of merely 1.5¹². Finding a more efficient pathway to achieve this separation is clearly one of the main objectives in current research in the area of chemical separation³. A very promising alternative is based on the *quantum sieving* effect, proposed by Beenakker *et al*¹³. This phenomenon is a consequence

the mass difference between H_2 and D_2 : a lower mass increases the zero-point energy of the internuclear bond, which in turn results in a more diffuse wave function and therefore a larger *effective size*. Thus, H_2 has a larger effective size when compared with the heavier D_2 . This size difference becomes critical when the molecules enter nanometric cavities, and can affect both their adsorption and diffusion properties. In the last two decades, the adsorption of H_2 and D_2 has been studied in several nanoporous materials such as carbon nanotubes^{14–16}, zeolites^{17,18}, or metal–organic frameworks (MOFs)^{19–23} with the aim of finding the best candidate for isotopic separation of H_2 and D_2 ; see also Ref 24 and references therein. Very recently, specifically tailored organic cage molecules have been reported to obtain selectivities of up to 8 by combining small pores connecting large cavities²⁵.

When studying quantum sieving, one has to distinguish between the change of the adsorption and diffusion properties of the adsorbates. In the former case, a heavier isotopologue is preferentially adsorbed in the nanomaterial (*thermodynamic* or *chemical affinity* quantum sieving), which can be straightforwardly interpreted through the relative change in ZPE of the two species when entering the nanometric cavity. Regarding diffusion, it is known that there are two competing quantum effects which simultaneously play a role in the process: on one hand, the ZPE effects described above decrease the diffusion barrier for the heavier deuterium, resulting in a higher mobility than expected. This effect has been claimed to result in an *inverse kinetic isotope effect*, namely, a faster diffusion of deuterium in nanoporous materials, compared with hydrogen^{26–28}. However, these studies were based on semiclassical Transition State Theory simulations, which neglect the second quantum effect: resonant tunneling, which has been seen to enhance hydrogen transport properties in systems such as carbon nanotubes²⁹. In this work we present converged quantum dynamics results considering all confinement effects for both H_2 and D_2 , from which we derive diffusion rates for both molecules in the low pressure regime. Due to the very large propagation times required to converge the diffusion probabilities (as a consequence of the low corrugation of the Potential Energy Surface along the diffusion coordinate), we use an adiabatic approximation to

the wave function described in a previous work from us²⁹ in order to increase the numerical performance of the propagations, without compromising the model’s accuracy.

2 Theoretical Methods

2.1 Diffusion coefficient calculation

In the low-pressure regime, the diffusion of a substance in a material can be modeled as a set of uncorrelated jumps between neighboring adsorption sites^{30,31}. From this perspective, the diffusion rate is obtained through:

$$D_{diff} = \frac{1}{2d} \sum_{j \neq i} k_{i \rightarrow j}(T) l_{i \rightarrow j}^2, \quad (1)$$

where $l_{i \rightarrow j}$ stands for the distance between two adsorption sites, $k_{i \rightarrow j}$ is the frequency of the jumps between them, and d is the dimensionality of the system (1 in this case). Eq. (1) implies that the adsorption sites are stable enough for the different DOFs of the system to thermalize between each jump. If the temperature is low enough, one can further simplify the previous equation to account only for the jumps between adjacent adsorption sites, which will dominate the process. The expression then reads:

$$D_{diff} = \frac{l^2}{2d} k_{hop}(T). \quad (2)$$

The problem of calculating the diffusion coefficient is then reduced to the calculation of the hopping probability between two adjacent adsorption sites. Following Zhang and Light³², this probability will be calculated through the flux–correlation function approach in a quantum dynamics formalism, which is summarized below.

The general expression for a transition rate is given by the thermal average of the Cumulative Reaction Probability (CRP), $N(E)$, which gives us the probability that the system

has to go from any reactant state to any product state, as a function of the energy. Then, assuming a Boltzmann distribution for the energy of the system, we have:

$$k(T) = \frac{1}{2\pi Q(T)} \int_{-\infty}^{\infty} e^{-\beta E} N(E) dE. \quad (3)$$

In the previous equation, $\beta = \frac{1}{k_B T}$, and $Q(T)$ is the partition function of the system defined as:

$$Q(T) = Tr(e^{\beta \hat{H}^{5D}}) q_z(T) \quad (4)$$

with $q_z(T) = L \left(\frac{mT}{2\pi} \right)^{\frac{1}{2}}$ the semiclassical partition function of a particle in a periodic potential and \hat{H}^{5D} the Hamiltonian of the *confined coordinates* of the system (see below). Finally, we use the flux–correlation functions approach^{33–35} to compute $N(E)$, as implemented in Refs 36,37. In this approach one sets a dividing surface, h , which separates reactants from products and defines the thermal flux operator across such a surface as $\hat{F}_{T_0} = e^{-\beta_0 \hat{H}/2} i[\hat{H}, h] e^{-\beta_0 \hat{H}/2}$, with $\beta = 1/k_B T_0$. The eigenvalues and eigenstates of this operator (f_{T_0} and $|f_{T_0}\rangle$, respectively) are obtained by iterative diagonalization and then propagated in real time to compute a flux correlation function, $C_{ff}(t) = \sum_{m,n} f_m f_n \langle f_n | e^{-i\hat{H}t} | f_m \rangle$. In this work we have used the State-Averaged variant of the Multiconfigurational Time–dependent Hartree (SA-MCTDH)³⁷ for both the iterative diagonalization of the different operators, and for the simultaneous propagation of the resulting wavepackets. The CRP is finally obtained by Fourier transform of $C_{ff}(t)$:

$$N(E) = \frac{1}{2} e^{2\beta_0 E} \sum_n \sum_m f_n f_m \left| \int_{-\infty}^{\infty} dt e^{iEt} \langle f_n | e^{-i\hat{H}t} | f_m \rangle \right|^2. \quad (5)$$

2.2 Modelization of the system

In order to compute the transition rate in Eq. 3, we modelled a single H₂ (or D₂) molecule in the hollow cavity of a carbon nanotube using its 3 internal degrees of freedom (ρ, θ, ϕ) as well as the 3 translational DOFs of the molecular center of mass (x, y, z) as a coordinate

system. This representation has been previously used by ourselves^{29,38,39} as well as by other authors^{15,40}. The quantum dynamics calculations were carried out using an adiabatic approximation, as described in a previous publication²⁹. Following such model we were able to solve the dynamics of a 1D wavepacket on a set of particular potential energy surfaces instead of propagating a full 6D function. The approximation is justified in terms of a time-scale separation argument between the large-amplitude motion of the molecule along the axis of the nanotube (z) and the fast motion on the *confined* coordinates (vibration, rotation, and translation in the xy plane; collectively referred to as q). The molecular wave packet evolves, thus, according to the 1D Time-dependent Schrödinger Equation (note that atomic units are used throughout this paper, and therefore $\hbar = 1$):

$$i\frac{\partial}{\partial t}\tilde{\psi}_j(z,t) = \hat{H}_j^{(ad)}\tilde{\psi}_j(z,t), \quad (6)$$

with the adiabatic Hamiltonian defined as:

$$\hat{H}_j^{(ad)} = \frac{1}{2m}\frac{\partial^2}{\partial z^2}z + \sum_{k=1}^{N_z}\varepsilon_j(z_k)|z_k\rangle\langle z_k| \quad (7)$$

Here, each function $\varepsilon_j(z_k)$ represents the z -dependent eigenvalue of a given eigenstate $\xi_j^{5D}(q; z_k)$ of the confined coordinates Hamiltonian, $\hat{H}^{5D}(q, z_k)$, and acts effectively as a potential energy term for the motion of the wave packet along the z dimension. We will hence refer to each $\varepsilon_j(z_k)$ as a *confined eigenstate potential energy surface* (cePES). To obtain them, we diagonalize the Hamiltonian of the confined coordinates at different points along the z axis; each z -dependent eigenvalue then conforms a given cePES.

In a previous work we proved that this adiabatic representation yields excellent agreement with full-dimensional propagations of the same system, while drastically reducing the computational effort. For details on the derivation and the model of the 5D eigenstates, we refer the reader to Ref. 29.

3 Results and discussion

3.1 Confined Eigenstates Potential Energy Surfaces

As a first step to study the diffusion, we took advantage of the adiabatic approach to visualize the diffusion process as a 1D problem. By observing the computed cePES we can obtain relevant information on the diffusion mechanism even before running actual quantum dynamics simulations of that process.

The SA-MCTDH approach was used to compute the eigenstates of the 5D Hamiltonian at the center of a unit cell of the nanotube ($z = 0$) via iterative diagonalization, using the wave function representation parameters given in Table 1. The 50 lowest energy eigenstates,

Table 1: Primitive and SPF basis sets for the calculation of the eigenstates of the 5D Hamiltonian for both H₂ and D₂. Distances given in Bohr radii, angles in radians. The same primitive basis was used for both isotopologues.

DOF	Number of SPFs		Primitive grid		
	H ₂	D ₂	Num. Points	Type	Range
ρ	2	2	32	FFT	0.5–5.0
θ	5	5	64	cot-DVR	$0-\pi/2$
ϕ	7	7	64	FFT	$0-2\pi$
x	3	4	32	FFT	-3.5–3.5
y	3	4	32	FFT	-3.5–3.5

$\xi_j^{5D}(q; z)$, were used as a basis for the matrix representation of \hat{H}^{5D} at 512 equispaced points along the z coordinate, extending from -56.1 to 56.1 Bohr radii which corresponds to 14 unit cells of the SWCNT. The total number of carbon atoms used to define the interaction potential was large enough to ensure that no edge effects were noticeable at the ends of the simulation grid.

The lower energy cePES corresponding to the H₂ molecule are depicted in the left panel of Figure 1. The different curves are drawn according to the *ortho-para* symmetry of the 5D eigenstate they represent: the solid, darker lines label a symmetric state and the dashed, lighter lines label an antisymmetric state. The same scheme is followed in the right panel, which shows the curves for D₂. From these figures we can extract an approximate value

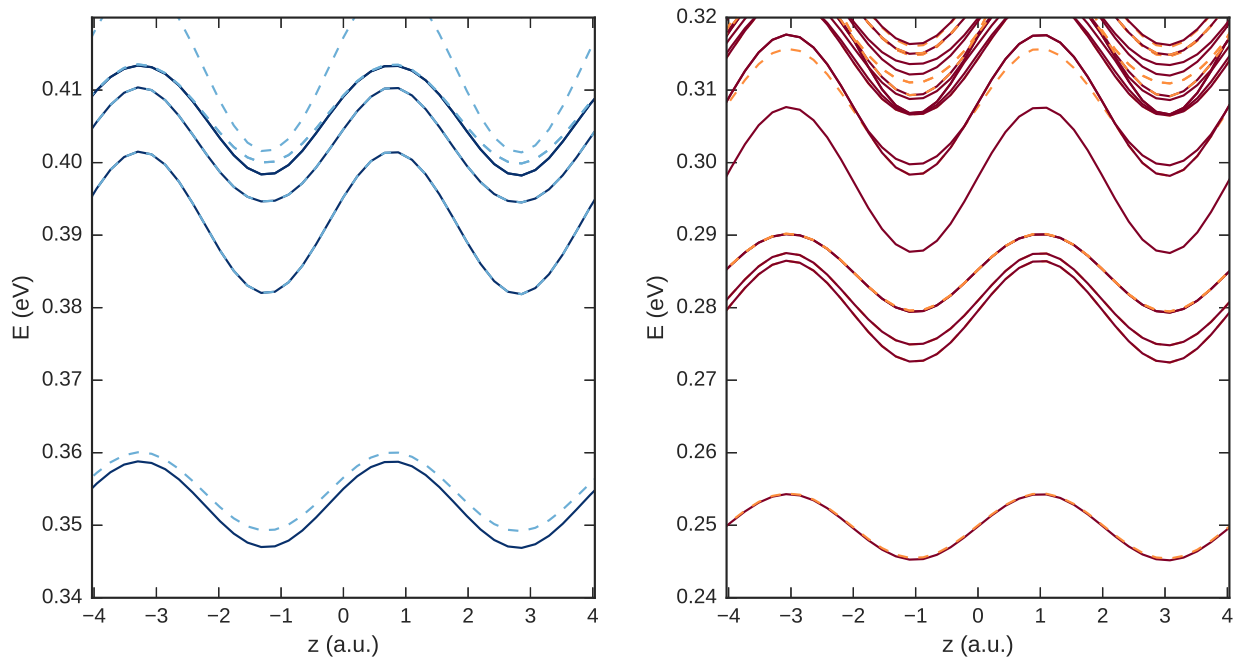


Figure 1: Variation along a single unit cell of the eigenenergies of the 5D hydrogen (left) and deuterium (right) eigenstates (cePES). Symmetric eigenstates with respect to inversion are represented with solid lines, while dashed lines label asymmetric states.

of the threshold energy, which is the minimum energy (including ZPE) the particle would need to go from reactants to products. This quantity corresponds to the maximum of the lowest-energy cePES, and has a value of $E_{tr} = 0.3588$ eV for H_2 , while for D_2 it decreases to $E_{tr} = 0.2543$ eV. The adiabatic diffusion barrier, ΔE_{tr} , defined as the difference between the maximum and the minimum of each cePES, is also slightly lower for D_2 (5.6 meV) than for H_2 (7.2 meV). A final feature is the density of confined eigenstates that each molecule presents. We can use the relation between flux eigenstates and the vibrational states of the transition complex to estimate how many eigenstates will contribute to the diffusion for a given energy range from the Boltzmann population of the vibrational levels of the molecule fixed at a point along the diffusion coordinate. It is readily seen that the spectrum is denser for D_2 than for H_2 , as a consequence of its larger mass, and therefore more eigenstates will contribute to the diffusion for D_2 than for H_2 .

All the effects presented in this section are directly or indirectly related to the different ZPE of the isotopologues, and point to the direction that, in confined environments, D_2 could diffuse faster than the lighter H_2 . This *inverse kinetic isotope effect* has been described previously in Carbon Molecular Sieves^{26,28,41–43} and nanotubes³⁹, and justified as a purely ZPE effect: due to the lower ZPE of D_2 its effective size is smaller than that of H_2 , and as a consequence the heavier isotopologue feels less the corrugation of the potential generated by the Carbon atoms, thus diffusing more easily than H_2 . In the next section, we will investigate if this effect persists when including all possible quantum effects via time-dependent simulation of the system.

3.2 Flux Correlation Functions and Cumulative reaction probability

As outlined above, we used the flux correlation functions approach together with the SAMCTDH method to compute the cumulative reaction probability. Since quantum effects are more relevant at lower temperatures, we set a value of β corresponding to 100 K, which yields

numerically stable results for $N(E)$ in the range of 40 to 125 K. The qualitative analysis of the cePES above allowed us to estimate that only 6 to 8 states have a significant population at the maximum temperature considered, and therefore contribute appreciably to $k(T)$. To ensure convergence of the calculations we chose to compute 26 flux eigenstates to represent the diffusion process of the H_2 molecule, and 30 in case of D_2 . The basis set used for both cases is described in Table 2.

Table 2: Primitive and SPF representation used in the flux eigenstates calculation and propagation.

DOF	Number of SPFs		Num. Points	Primitive grid	
	H_2	D_2		Type	Range
q	20	14	50	Discrete	–
z	20	20	512	FFT	$-56.066 - 56.066 a_0$

The resulting flux states were propagated for a total time of 20 ps, using again the SA-MCTDH method. To prevent transmissions and reflections in the edge of the representation grid we added a transmission-free complex absorbing potential (CAP) as defined by Manolopoulos^{44,45} with a length of 20 bohr. The transmission-free nature of the CAP was required due to the existence of long-lived processes in the diffusion mechanism (See below, and Ref. 29, for details on these processes).

The integral of C_{ff} over time t , known as the *flux-position correlation function*, $C_{fp}(t)$, can be used as a rule of thumb to estimate the convergence of a calculation: the value of this quantity stabilizes as the wave packet leaves the interaction region, and it reaches a plateau once the amplitude of the function in that region becomes zero. Therefore, to obtain a perfectly converged CRP one has to choose a propagation time T such that a constant value of $C_{fp}(t)$ is achieved for any time $t > T$. The flux-position correlation functions obtained after a total propagation time of 20 ps for H_2 and D_2 are shown in the left and right panel of Figure 2, respectively.

For the long time propagations reported in this work, note that in neither case does the function admittedly reach a constant value, thus indicating that a portion of the wave

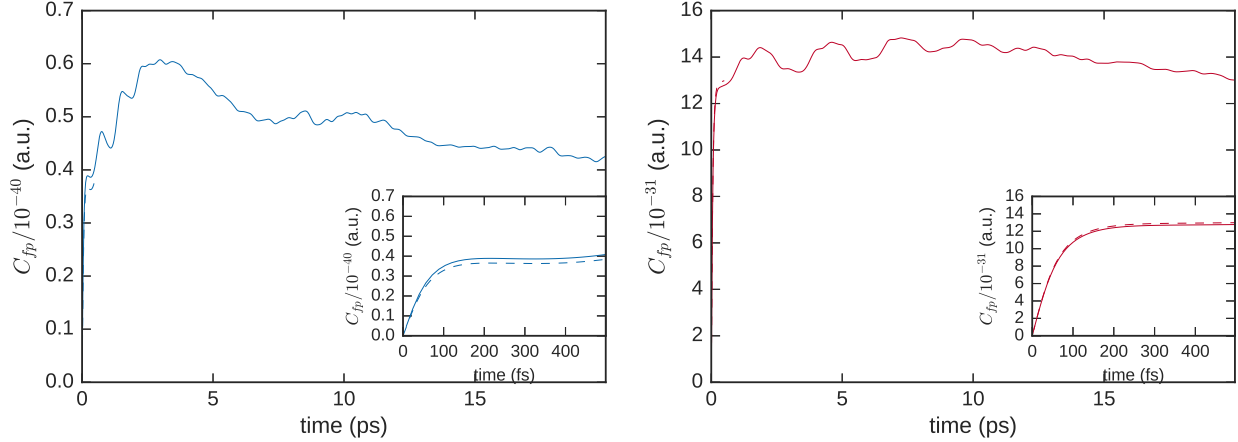


Figure 2: Flux–position correlation function for the diffusion of H₂ (right) and D₂ (left) along an (8,0) SWCNT. Inset: close up to the short–time region (dashed line corresponding to the 6D propagation in Ref. 39).

packets is still in the interaction region even after 20 ps. This is a direct consequence of the small barrier for the diffusion process. Additionally, the fine structure of the functions is also a signal of the presence of resonances in the diffusion process²⁹. These two features of the system would enforce us to go to much longer times to obtain a perfectly converged CRP. However, this time would only contribute to the resolution of the resonances, at the price of more computational effort and potential numerical instability. Instead of increasing the propagation time, we multiplied $C_{ff}(t)$ by a Gaussian convolution function with $\Delta E = 0.12$ meV to reduce the aliasing coming from the truncation of the Fourier Transform in Eq. 5²⁹.

The resulting $N(E)$ for H₂ and D₂ are shown in Figures 3 and 4, respectively, together with the individual contributions of the lowest–energy flux eigenstates. Additionally, the threshold energy for the diffusion process is marked in both figures as a dashed vertical line.

The first feature to notice in both plots is their significant amount of fine structure in form of sharp peaks. In a previous work²⁹ these features were confirmed to be shape and Feshbah resonances by calculating the exact 6D eigenstates of H₂ in a unit cell of the carbon nanotube using periodic boundary conditions, and checking that the energies of the

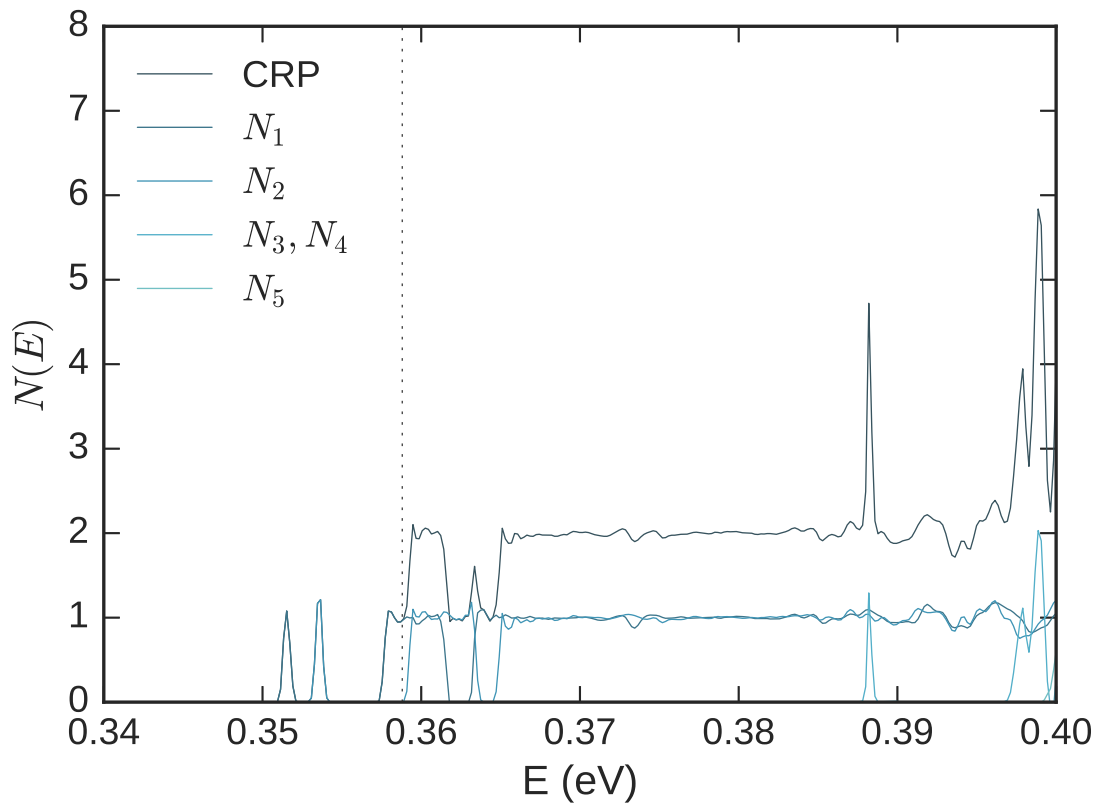


Figure 3: Cumulative Reaction Probability and individual flux eigenstates contributions for the diffusion of H_2 after 20 ps propagation. Vertical dotted lines marks the diffusion energy threshold.

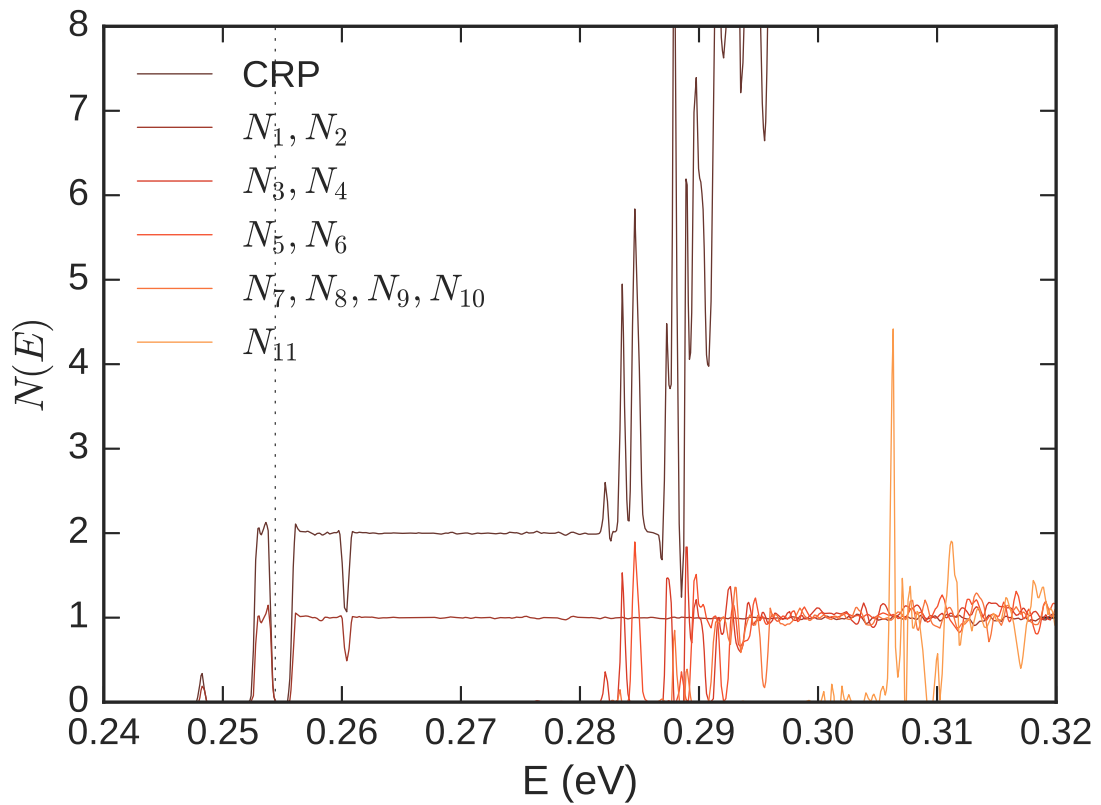


Figure 4: Cumulative Reaction Probability and individual flux eigenstates contributions for the diffusion of D_2 after 20 ps propagation. Vertical dotted lines marks the diffusion energy threshold.

peaks coincide with the eigenvalues of the tunneling 6D states. Moreover, the width of the peaks is consistent with the tunneling splitting of the resonant state, which further confirms the accuracy of the propagation. The large amount of resonant states is consistent with the shape of $C_{fp}(t)$ discussed previously, as the low-energy resonances provide a way for the wave packet to enter and leave the interaction region easily. More importantly, some resonances are found at energies below the diffusion threshold for both isotopologues, indicating that tunneling effect is relevant for the diffusion process at low temperatures.

Comparing the cumulative reaction probability curves for both H₂ and D₂, one can see two main differences: on one hand, the energy and intensity of the first resonances; on the other, the density of the higher energy resonances. The former is probably the more critical point, since this difference will influence more heavily the behavior of the different molecules at very low temperature. The two first resonances in $N(E)$ for the H₂ molecule are both intense and appear at energies significantly lower than the threshold. Moreover, a second-order resonance appears at $E = 0.36$ eV, just above the diffusion threshold, thus contributing to increase the diffusion rate at all temperatures. On the contrary, for D₂ we have a quite negligible resonance at $E = 0.248$ eV, while two strong resonances exist at energies just below the energy threshold. Being so close to the diffusion threshold, these resonances will have a smaller effect on D_{diff} than those present in H₂ at low temperatures. Similarly, even though D₂ presents a denser resonance spectrum than H₂ at high energies, these do not play any role in the diffusion process in the studied temperature range, since the resonant states are too energetic to have significant population.

Once we analyzed $N(E)$ thoroughly, the transition coefficient was obtained by Boltzmann averaging of the CRP at different temperatures, and then inserted in Eq (1) to compute the diffusion rate. The diffusion coefficient is plotted in Figure 5 as a function of temperature inverse for both H₂ and D₂ as solid blue and red lines, respectively. The same quantities have been computed using a Transition State Theory (TST) model, and are also shown in the same figure as dotted lines. The sum of all the quantum effects outlined previously (*i.e.* ZPE

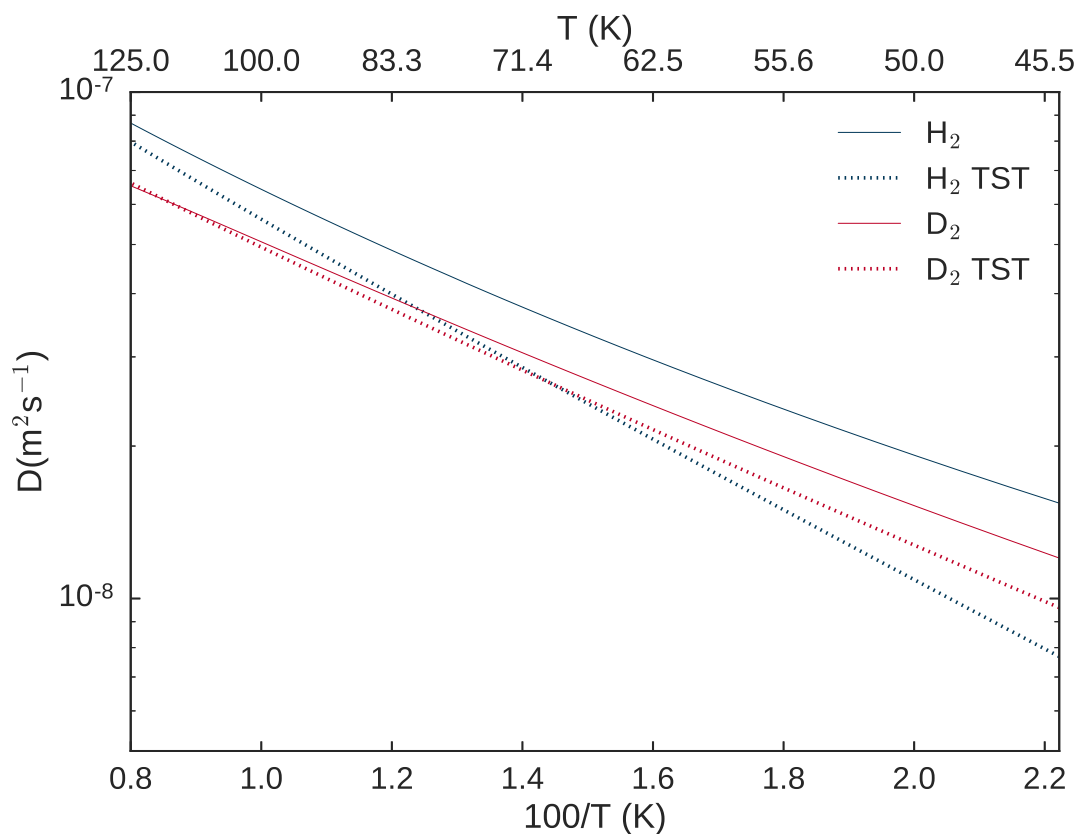


Figure 5: Diffusion rates for H₂ (blue) and D₂ (red) computed with the flux correlation function approach (solid lines) and with TST (dotted lines).

effects and tunneling) significantly changes the diffusion rates with respect to those predicted by simple TST calculations. It is readily seen that there is a relevant increase of D_{diff} at low temperatures for both isotopologues, but more so for the lighter H_2 , as it was expected from the discussion of the cumulative reaction probability above. In fact, some tunneling contributions remains at temperatures as high as 125 K for this molecule. The consequence of the different amount of tunneling effect for both species is important even qualitatively: TST predicts a turnover of the diffusion rates at temperatures below 70 K, with D_2 starting to diffuse faster than H_2 at this point. This inverse Kinetic Isotope Effect is consistent with the discussion of the adiabatic diffusion barrier discussed Section 3.1 and widely studied in Carbon Molecular Sieves. In a previous work³⁹ we reported that the same effect would be observed for the diffusion of H_2 and D_2 along SWCNTs, and supported such a claim with quantum dynamics simulations of the full 6D system up to 500 fs. The current results change dramatically the conclusions of that work: it is now clear that 500 fs propagations resulted in insufficiently converged $N(E)$, which did not properly resolve the resonances and gravely underestimated tunneling contributions. With the correctly converged cumulative reaction probability and the resonances properly resolved, tunneling outweighs the ZPE effects at low temperatures, and the inverse kinetic isotope effect does not take place. This results shows the importance of an accurate quantum mechanical description of H_2 and D_2 when studying their diffusion properties.

4 Summary and Conclusions

The calculation of the diffusion rates for H_2 and D_2 along a (8,0) CNT in the low pressure limit has been carried out using the single-hopping approach. The hopping rate was obtained through the general expression of a transmission rate, with the cumulative reaction probability computed with the flux-correlation function approach. In order to achieve convergence of $N(E)$, we used an adiabaticization scheme to reduce the problem from a 6D Hamiltonian

to a 2D system, thus being able to propagate the flux eigenstates for 20 ps. This allowed us to resolve resonant structures in $N(E)$ which enhance diffusion at low temperatures.

The diffusion rates calculated in this work differ from previous studies in that no inverse kinetic isotope effect appears in this particular system. This qualitative inconsistency with a previous work of us indicates that $N(E)$ was not correctly converged in those calculations. The difference with other theoretical and experimental studies on other nanostructured materials like Carbon Molecular Sieves, however, is probably due to the different structure of those, which present large pores connected through narrow channels rather than the cylindrical shape of carbon nanotubes. Despite this fundamental difference, the behavior of the molecules inside a carbon nanotube can be used to model the transport within the narrow channels connecting pores in other nanomaterials, or to consider the design of new devices based purely on nanotubes.

5 Acknowledgements

Financial support from the Spanish Ministerio de Economía y Competitividad (Ministry of Economy and Competitiveness) (CTQ2013-41307-P) and Generalitat de Catalunya (2014-SGR-25) is acknowledged. M.M.-M. further thanks a predoctoral grant from the FPU program (FPU2013/02210) from the Spanish Ministerio de Educación, Cultura y Deporte (Ministry of Education, Culture and Sports).

References

- (1) Dunn, S. Hydrogen Futures: Toward a Sustainable Energy System. *International Journal of Hydrogen Energy* **2002**, *27*, 235–264.
- (2) Schlapbach, L.; Züttel, A. Hydrogen-Storage Materials for Mobile Applications. *Nature* **2001**, *414*, 353–358.

- (3) Basile, A. B., Dalena, F. D., Jianhua Tong, J. T., Vezirolu, T. N. V., Eds. *Hydrogen Production, Separation and Purification for Energy*; Institution of Engineering and Technology, 2017.
- (4) Stiopkin, I. V.; Weeraman, C.; Pieniazek, P. A.; Shalhout, F. Y.; Skinner, J. L.; Benderskii, A. V. Hydrogen Bonding at the Water Surface Revealed by Isotopic Dilution Spectroscopy. *Nature* **2011**, *474*, 192–195.
- (5) Mantsch, H. H.; Saitô, H.; Smith, I. C. Deuterium Magnetic Resonance, Applications in Chemistry, Physics and Biology. *Progress in Nuclear Magnetic Resonance Spectroscopy* **1977**, *11*, 211–272.
- (6) Ewanicki, J.; Kim, W.; Wang, W. 2H SOLSOR: A Novel Tool for Reducing Volume Variation as a Source of Error in External Standard Quantitative NMR. *Magnetic Resonance in Chemistry* **2020**, *58*, 733–744.
- (7) Büldt, G.; Gally, H. U.; Seelig, A.; Seelig, J.; Zaccari, G. Neutron Diffraction Studies on Selectively Deuterated Phospholipid Bilayers. *Nature* **1978**, *271*, 182–184.
- (8) Liebschner, D.; Afonine, P. V.; Moriarty, N. W.; Langan, P.; Adams, P. D. Evaluation of Models Determined by Neutron Diffraction and Proposed Improvements to their Validation and Deposition. *Acta Crystallographica Section D: Structural Biology* **2018**, *74*, 800–813.
- (9) About — Center for Gas Separations. <http://www.cchem.berkeley.edu/co2efrc/about.html>.
- (10) *Handbook of Nuclear Chemistry*; Springer US: Boston, MA, 2003; pp 1863–1897.
- (11) Spindel, W.; Ishida, T. Isotope Separation. *Journal of Chemical Education* **1991**, *68*, 312–318.
- (12) Rae, H. K. In *Separation of Hydrogen Isotopes*; Rae, H. K., Ed.; UTC, 1978; Vol. 10; pp 1–26.

- (13) Beenakker, J. J. M.; Borman, V. D.; Krylov, S. Y. Molecular Transport in the Nanometer Regime. *Physical Review Letters* **1994**, *72*, 514–517.
- (14) Wang, Q.; Challa, S.; Sholl, D.; Johnson, J. Quantum Sieving in Carbon Nanotubes and Zeolites. *Physical Review Letters* **1999**, *82*, 956–959.
- (15) Lu, T.; Goldfield, E. E. M.; Gray, S. S. K. Quantum States of Hydrogen and Its Isotopes Confined in Single-Walled Carbon Nanotubes: Dependence on Interaction Potential and Extreme Two-dimensional Confinement. *Journal of Physical Chemistry B* **2006**, *110*, 1742–1751.
- (16) Garberoglio, G. Quantum Sieving in Organic Frameworks. *Chemical Physics Letters* **2009**, *467*, 270–275.
- (17) De Luca, G. Gusev and Suter Calculation of the Diffusion Coefficients of Light Gases in Silicalite-1 Membrane and Silica-Sodalite Zeolite. *Separation and Purification Technology* **2004**, *36*, 215–228.
- (18) Salazar, J. M.; Badawi, M.; Radola, B.; Macaud, M.; Simon, J. M. Quantum Effects on the Diffusivity of Hydrogen Isotopes in Zeolites. *Journal of Physical Chemistry C* **2019**, *123*, 23455–23463.
- (19) Oh, H.; Hirscher, M.; Separation, H. I. Quantum Sieving for Separation of Hydrogen Isotopes Using MOFs. *European Journal of Inorganic Chemistry* **2016**, *2016*, 4278–4289.
- (20) FitzGerald, S. A.; Allen, K.; Landerman, P.; Hopkins, J.; Matters, J.; Myers, R.; Rowsell, J. L. Quantum Dynamics of Adsorbed H₂ in the Microporous Framework MOF-5 Analyzed Using Diffuse Reflectance Infrared Spectroscopy. *Physical Review B - Condensed Matter and Materials Physics* **2008**, *77*, 224301.

- (21) Kim, J. Y.; Balderas-Xicohténcatl, R.; Zhang, L.; Kang, S. G.; Hirscher, M.; Oh, H.; Moon, H. R. Exploiting Diffusion Barrier and Chemical Affinity of Metal–organic Frameworks for Efficient Hydrogen Isotope Separation. *Journal of the American Chemical Society* **2017**, *139*, 15135–15141.
- (22) Fitzgerald, S. A.; Shinbrough, K.; Rigdon, K. H.; Rowsell, J. L.; Kapelewski, M. T.; Pang, S. H.; Lawler, K. V.; Forster, P. M. Temperature-Programmed Desorption for Isotope Separation in Nanoporous Materials. *Journal of Physical Chemistry C* **2018**, *122*, 1995–2001.
- (23) Radola, B.; Giraudet, M.; Bezverkhyy, I.; Simon, J. M.; Salazar, M.; Macaud, M.; Bellat, J. P. New Force Field for GCMC Simulation of D₂/H₂ Quantum Sieving in Pure Silica Zeolites. *Physical Chemistry Chemical Physics* **2020**,
- (24) Kim, J. Y.; Oh, H.; Moon, H. R. Hydrogen Isotope Separation in Confined Nanospaces: Carbons, Zeolites, Metal–organic Frameworks, and Covalent Organic Frameworks. *Advanced Materials* **2019**, *31*, 1805293.
- (25) Liu, M.; Zhang, L.; Little, M. A.; Kapil, V.; Ceriotti, M.; Yang, S.; Ding, L.; Holden, D. L.; Balderas-Xicohténcatl, R.; He, D. et al. Barely Porous Organic Cages for Hydrogen Isotope Separation. *Science* **2019**, *366*, 613–620.
- (26) Kumar, A. V. A.; Bhatia, S. K. Quantum Effect Induced Reverse Kinetic Molecular Sieving in Microporous Materials. *Physical Review Letters* **2005**, *95*, 1–4.
- (27) Kumar, A. V. A.; Jobic, H.; Bhatia, S. K. Quantum Effects on Adsorption and Diffusion Of Hydrogen and Deuterium in Microporous Materials. *Journal of Physical Chemistry B* **2006**, *110*, 16666–71.
- (28) Kumar, A. V. A.; Bhatia, S. K. Is Kinetic Molecular Sieving of Hydrogen Isotopes Feasible? *Journal of Physical Chemistry C* **2008**, *112*, 11421–11426.

- (29) Mondelo-Martell, M.; Huarte-Larrañaga, F.; Manthe, U. Quantum Dynamics of H₂ in A Carbon Nanotube: Separation of Time Scales and Resonance Enhanced Tunneling. *Journal of Chemical Physics* **2017**, *147*, 084103.
- (30) Doll, J. D.; Voter, A. F. Recent Developments in the Theory of Surface Diffusion. *Annual Review of Physical Chemistry* **1987**, *38*, 413–431.
- (31) Barth, J. Transport of Adsorbates At Metal Surfaces: From Thermal Migration To Hot Precursors. *Surface Science Reports* **2000**, *40*, 75–149.
- (32) Zhang, D. H.; Light, J. C.; Lee, S.-Y. Y. Transition State Wave Packet Study of Hydrogen Diffusion on Cu(100) Surface. *Journal of Chemical Physics* **1999**, *111*, 5741–5753.
- (33) Yamamoto, T. Quantum Statistical Mechanical Theory of the Rate of Exchange Chemical Reactions in the Gas Phase. *Journal of Chemical Physics* **1960**, *33*, 281.
- (34) Miller, W. H. Quantum Mechanical Transition State Theory and a New Semiclassical Model for Reaction Rate Constants. *Journal of Chemical Physics* **1974**, *61*, 1823–1834.
- (35) Miller, W. H.; Schwartz, S. D.; Tromp, J. W. Quantum Mechanical Rate Constants for Bimolecular Reactions. *Journal of Chemical Physics* **1983**, *79*, 4889–4898.
- (36) Matzkies, F.; Manthe, U. Accurate Quantum Calculations of Thermal Rate Constants Employing MCTDH: H₂+OH → H+H₂O and D₂+O → HD+DOH. *Journal of Chemical Physics* **1998**, *108*, 4828.
- (37) Manthe, U. The State Averaged Multiconfigurational Time-Dependent Hartree Approach: Vibrational State and Reaction Rate Calculations. *Journal of Chemical Physics* **2008**, *128*, 64108–12.
- (38) Mondelo-Martell, M.; Huarte-Larrañaga, F. Quantum Dynamics Study of the H₂ Molecule Confined in Single-Walled Carbon Nanotubes. *Journal of Physics: Conference Series* **2015**, *635*, 032057.

- (39) Mondelo-Martell, M.; Huarte-Larrañaga, F. Diffusion of H₂ and D₂ Confined in Single-Walled Carbon Nanotubes: Quantum Dynamics and Confinement Effects. *Journal of Physical Chemistry A* **2016**, *120*, 6501–6512.
- (40) Garberoglio, G.; DeKlavon, M. M.; Johnson, J. K. Quantum Sieving in Single-Walled Carbon Nanotubes: Effect of Interaction Potential and Rotational-translational Coupling. *Journal of Physical Chemistry B* **2006**, *110*, 1733–1741.
- (41) Nguyen, T. X.; Jobic, H.; Bhatia, S. K. Microscopic Observation of Kinetic Molecular Sieving of Hydrogen Isotopes in a Nanoporous Material. *Physical Review Letters* **2010**, *105*, 085901.
- (42) Hankel, M.; Zhang, H.; Nguyen, T. X.; Bhatia, S. K.; Gray, S. K.; Smith, S. C. Kinetic Modelling of Molecular Hydrogen Transport in Microporous Carbon Materials. *Physical Chemistry Chemical Physics* **2011**, *13*, 7834–44.
- (43) Contescu, C. I.; Zhang, H.; Olsen, R. J.; Mamontov, E.; Morris, J. R.; Gallego, N. C. Isotope Effect on Adsorbed Quantum Phases: Diffusion of H₂ and D₂ in Nanoporous Carbon. *Physical Review Letters* **2013**, *110*, 236102–5.
- (44) Manolopoulos, D. E. Derivation and Reflection Properties of a Transmission-Free Absorbing Potential. *Journal of Chemical Physics* **2002**, *117*, 9552–9559.
- (45) Gonzalez-Lezana, T.; Rackham, E. J.; Manolopoulos, D. E. Quantum Reactive Scattering with a Transmission-Free Absorbing Potential. *Journal of Chemical Physics* **2004**, *120*, 2247–2254.

Graphical TOC Entry

